

Copper homeostasis at the host vibrio interface: lessons from intracellular vibrio transcriptomics

A.S. Vanhove, T.P. Rubio, A.N. Nguyen, A. Lemire, D. Roche, J. Nicod, Agnès Vergnes, Aurore Poirier, E. Disconzi, Evelyne Bachère, et al.

▶ **To cite this version:**

A.S. Vanhove, T.P. Rubio, A.N. Nguyen, A. Lemire, D. Roche, et al.. Copper homeostasis at the host vibrio interface: lessons from intracellular vibrio transcriptomics. Environmental Microbiology, 2016, Pathogen Ecology, 18 (3), pp.875-888. 10.1111/1462-2920.13083 . hal-01311061

HAL Id: hal-01311061
https://sde.hal.science/hal-01311061

Submitted on 2 Feb 2021

HAL is a multi-disciplinary open access archive for the deposit and dissemination of scientific research documents, whether they are published or not. The documents may come from teaching and research institutions in France or abroad, or from public or private research centers.

L'archive ouverte pluridisciplinaire **HAL**, est destinée au dépôt et à la diffusion de documents scientifiques de niveau recherche, publiés ou non, émanant des établissements d'enseignement et de recherche français ou étrangers, des laboratoires publics ou privés.

Copper homeostasis at the host vibrio interface: lessons from intracellular vibrio transcriptomics

Audrey S. Vanhove,[1†] Tristan P. Rubio,[1†] An N. Nguyen,[2] Astrid Lemire,[3,4] David Roche,[5,6] Julie Nicod,[1] Agnès Vergnes,[1] Aurore C. Poirier,[1] Elena Disconzi,[2] Evelyne Bachère,[1] Frédérique Le Roux,[3,4] Annick Jacq,[2] Guillaume M. Charrière[1‡] and Delphine Destoumieux-Garzón[1*‡]

[1]*Interactions Hôtes-Pathogènes-Environnements (IHPE), UMR 5244, CNRS, Ifremer, Université de Perpignan Via Domitia, Université de Montpellier, Montpellier 34095, France.*

[2]*Institute for Integrative Biology of the Cell (I2BC), CEA, CNRS, Université Paris-Sud, Orsay Cedex 91405, France.*

[3]*Unité Physiologie Fonctionnelle des Organismes Marins, Ifremer, ZI de la Pointe du Diable, CS 10070, Plouzané 29280, France.*

[4]*UPMC Paris 06, CNRS, UMR 8227, Integrative Biology of Marine Models, Station Biologique de Roscoff, Sorbonne Université, CS 90074, Roscoff cedex 29688, France.*

[5]*Commissariat à l'Energie Atomique et aux Energies Alternatives (CEA), Direction des Sciences du Vivant (DSV), Institut de Génomique (IG), Génoscope, Evry cedex 91057, France.*

[6]*CNRS, UMR 8030, Laboratoire d'Analyse Bioinformatiques en Génomique et Métabolisme (LABGeM), Evry cedex 91057, France.*

[†]Audrey S. Vanhove and Tristan P. Rubio contributed equally in this study.

[‡]Guillaume M. Charrière and Delphine Destoumieux-Garzón contributed equally in this study

Corresponding author ddestoum@ ifremer.fr

Summary

Recent studies revealed that several vibrio species have evolved the capacity to survive inside host cells. However, it is still often ignored if intracellular stages are required for pathogenicity. Virulence of *Vibrio tasmaniensis* LGP32, a strain pathogenic for *Crassostrea gigas* oysters, depends on entry into hemocytes, the oyster immune cells. We investigated here the mechanisms of LGP32 intracellular survival and their consequences on the host–pathogen inter-action. Entry and survival inside hemocytes were required for LGP32-driven cytolysis of hemocytes, both *in vivo* and *in vitro*. LGP32 intracellular stages showed a profound boost in metabolic activity and a major transcription of antioxidant and copper detoxification genes, as revealed by RNA sequencing. LGP32 isogenic mutants showed that resistance to oxidative stress and copper efflux are two main functions required for vibrio intracellular stages and cytotoxicity to hemocytes. Copper efflux was also essential for host colonization and virulence *in vivo*. Altogether, our results identify copper resistance as a major mechanism to resist killing by phagocytes, induce cytolysis of immune cells and colonize oysters. Selection of such resistance traits could arise from vibrio interactions with copper-rich environmental niches including marine invertebrates, which favour the emergence of pathogenic vibrios resistant to intraphagosomal killing across animal species.

Introduction

Vibrios have long been considered extracellular organisms. However, an increasing number of studies show that some vibrio strains have evolved cell invasive properties. The capacity to survive in host cells was reported for vibrio strains pathogenic for humans. Examples include *Vibrio cholerae*, which survives in mouse cell lines (Duperthuy *et al*., 2010), and *V. parahaemolyticus*, which disrupts the intestinal epithelium (Ritchie *et al*., 2012) and can also invade and replicate in human HeLa cell line (Zhang *et al*., 2012; de Souza Santos and Orth, 2014). Interestingly, in a few animal species, such vibrio intracellular stages have been associated with diseases. For example, the coral pathogens *V. shiloi* (Rosenberg and Falkovitz, 2004) and *V. coralliilyticus* (Vidal-Dupiol *et al*., 2011) enter coral epithelial cells as part of their pathogenic process. Similarly, the oyster pathogen *V. tasmaniensis* LGP32 enters oyster immune cells, the hemocytes, and this is required for virulence in oysters (Duperthuy *et al*., 2011).

Survival in professional phagocytes requires evading or resisting the phagosome hostile environment. Multiple stresses are used by professional phagocytes to kill phagocytosed microorganisms (Flannagan *et al*., 2009).

The NADPH oxidase produces potent reactive oxygen species (ROS) which are delivered into the phagolysosome during its maturation together with a series of hydrolytic enzymes and antimicrobial peptides. Moreover, an acidic environment is created by accumulating protons in the lumen of the phagosome. This environment is both aggressive to the phagocytosed bacteria and optimal for the activity of the hydrolytic enzymes. Such microbicidal mechanisms are broadly conserved throughout evolution (Boulais *et al*., 2010) and they have been well described in oyster hemocytes (Bachere *et al*., 2015).

While vibrio intracellular stages have been associated with the expression of key virulence factors (Ma *et al*., 2009; Zhang *et al*., 2012), it is still often unknown whether those stages play an essential role in pathological processes induced by vibrios. In the *V. tasmaniensis* LGP32/ oyster interaction, where vibrios behave as facultative intravacuolar pathogens (Vanhove *et al*., 2015), a tight correlation has been found between entry into host immune cells and virulence in experimental infections (Duperthuy *et al*., 2010; 2011). We indeed previously showed (i) that the major outer membrane protein OmpU of LGP32 was required for efficient plasma opsonization, β-integrin recognition and subsequent entry into oyster hemocytes (Duperthuy *et al*., 2011) and (ii) that *ompU*deletion mutants were strongly attenuated in terms of virulence (Duperthuy *et al*., 2010). We also observed important cell damages in hemocytes heavily loaded with LGP32 (Vanhove *et al*., 2015), suggesting that phagocytosed LGP32 could be cytotoxic to oyster hemocytes. Supporting this hypothesis, some virulence factors were shown to be secreted by outer membrane vesicles released by LGP32 inside the phagosome (Vanhove *et al*., 2015). To the best of our knowledge, it is so far the only model in which invasion of professional phagocytes by vibrios has been so clearly associated

with disease expression *in vivo*. Therefore, this model offers a great opportunity to decipher the causal relationships between intracellular stages and virulence in vibrios and decipher the molecular bases of vibrio survival in the hostile environment of the phagosome.

Here, we took advantage of this model to characterize vibrio intracellular stages and identify key functions required for vibrio intracellular survival in immune cells. LGP32 cytotoxicity was found to depend upon entry and survival in oyster hemocytes. By comparative transcriptomics, we identified antioxidant responses and copper efflux as functions highly induced intracellularly. Their key role in intracellular survival and cytotoxicity to host immune cells was demonstrated genetically. Altogether, our results identify copper homeostasis as a key player in the vibrio/phagocyte interaction and copper efflux as a major vibrio adaptive trait for oyster tissue colonization and virulence in oyster experimental infections.

Results

Phagocytosis and intracellular survival of LGP32 are required to induce cytolysis

Characterization of the *V. tasmaniensis* strain LGP32/ hemocyte interactions at the cellular level was performed by infecting primary cultures of oyster hemocytes maintained in sterile sea water (SSW) with GFP-expressing strains opsonized in oyster plasma. Plasma-opsonized LGP32 grew significantly in hemocyte co-cultures ($P < 0.001$), unlike the phylogenically related LMG 20012^T (Thompson *et al*., 2003), an avirulent control strain used in our previous study (Duperthuy *et al*., 2011; Fig. 1A). However, plasma-opsonized LGP32 was unable to grow in SSW in the absence of hemocytes (Fig. 1A), which showed that hemocytes are required to support the growth of LGP32 in such a nutrient-poor environment. The hemocyte/vibrio interaction was then monitored over the first 5 h of contact by epifluorescence microscopy. After a 1 h contact, oyster hemocytes were already heavily loaded with either LGP32 or LMG 20012^T. After 3 h, most LGP32 were intravacuolar but some bacteria-containing hemocytes harbouring cellular alterations had lost adherence: they were found in the culture supernatant together with some extracellular vibrios. After 5 h, no more LGP32containing hemocytes were adherent; several hemocytes were present in the supernatant and most of the LGP32 were extracellular (Figs 1B, Supporting Information Fig. S1). On the contrary, LMG 20012^T remained within hemocytes over the course of the experiment without any sign of hemocyte alteration. Therefore, LGP32 entry into hemocytes triggers a loss of hemocyte integrity leading to the release of LGP32 through cytolysis ~5 h after phagocytosis.

To quantify the LGP32-induced cytolysis of hemocytes, we used the cell impermeant Sytox green DNA dye. In agreement with our microcopy data (Fig. 1B), 5 to 7 h after LGP32 phagocytosis, hemocyte monolayers generated a massive Sytox green fluorescent signal as opposed to LMG 20012^T ($P < 0.001$; Fig. 1C). Thus, alteration of hemocyte membrane integrity is observed after LGP32 phagocytosis. Remarkably, cytochalasin D, an inhibitor of F-actin polymerization that prevents phagocytosis, abolished LGP32-induced hemocyte cytolysis (Fig. 1C). We concluded that

cytotoxicity of LGP32 towards oyster hemocytes is strictly dependent on phagocytosis. Altogether, those results show that intracellular LGP32 resists to the hemocyte killing machinery, and within few hours becomes cytotoxic, thereby promoting a hemocyte cytolysis that could sustain its own growth.

Antioxidant responses and metal homeostasis genes are highly expressed intracellularly

To identify the mechanisms involved in LGP32 resistance to the hemocyte killing machinery and phagocytosisdependent cytotoxicity, we used a global comparative RNAseq approach early after vibrio entry into hemocytes
(1 h after phagocytosis). Transcripts of intracellular LGP32 were obtained from hemocyte monolayers and their relative level of expression was compared with that of transcripts of extracellular LGP32 obtained from vibrios kept in SSW alone. Out of 3230 genomic elements (not including rRNA genes), transcript levels of 1280 genes varied by more than fourfold in the intracellular condition, with a false detection rate of 5% in all triplicate conditions (Supporting Information Table S1; GEO Submission GSE73260). The RNAseq results were validated by qRTPCR for 84% of the tested genes on another set of three independent experiments (Supporting Information Fig. S2). RNAseq revealed a massive activation of LGP32 metabolism inside the hemocytes. Indeed, the three functional categories that gathered most of the differentially expressed genes were *protein synthesis*, *carbon compound utilization and transport*, and *amino acid transport and metabolism*. An important up-regulation of genes involved in *glycogenesis*, *gluconeogenesis*, *TCA cycle*, as well as in *envelope*, *LPS and capsule biogenesis* was also observed (Supporting Information Table S1; Table 1).
Finally, *stress response* and *metal homeostasis* were functions highly impacted by the intracellular environment.

Copper efflux and antioxidant genes were the most highly induced in the intracellular environment. Indeed, among 34 genes overexpressed more than 50 times (i.e. 0.8% of the transcriptome; Table 2), five genes were involved in copper efflux: *cus*CBAF (VS_II0514, VS_II0515, VS_II0516, VS_II0517) and *cop*A (VS_0768), which encode a RND-transporter and a P-type ATPase respectively. Three additional genes were involved in the antioxidant response, namely *sodA* (VS_2918) and *ahpC*/ *ahpF* (VS_2126, VS_2127), which encode a superoxide dismutase and an alkyl hydroperoxide reductase complex respectively. As RNAseq was performed in whole hemolymph, we evaluated the respective role of plasma versus the intracellular environment on the expression of candidate genes. As a control, vibrios were incubated in SSW for the same times. While the antioxidant genes *ahpC* and *sodA* were induced only after entry into hemocytes ($P < 0.01$), copper efflux genes *copA* and *cusB* were already induced in oyster plasma ($P < 0.01$). Still, after 1 h, *copA* expression remained 20 times higher in the intracellular condition than in the extracellular controls ($P < 0.01$; Fig. 2).

The antioxidant sodA gene is required for intracellular

To determine whether the antioxidant response was necessary for LGP32 intracellular survival and phagocytosisdependent cytotoxicity, we constructed deletion mutants lacking *sodA* (VS_2918) and *ahpC* (VS_2126). As a second copy of *ahpC* (VS_2126) referred to as *tsa* (VS_0593) was found in LGP32 genome (39.8% amino acid identity), we also constructed a Δ*ahpC/tsa* double mutant. Deletions were confirmed by PCR and sequencing (Supporting Information Fig. S3). Growth in Zobell medium or plasma and phagocytosis efficiency did not significantly differ from the wild-type LGP32 (Supporting Information Figs S4 and S5). Interestingly, for Δ*sodA*, but not Δ*ahpC* nor Δ*ahpC/tsa* (Supporting Information Fig. S6), we observed a strongly attenuated phagocytosis-dependent growth ($P < 0.001$) and cytotoxicity ($P < 0.001$) compared with the wild-type LGP32 (Fig. 3A and B). Complementation of Δ*sodA* with pMRB plasmids encoding *sodA* led to a dose-dependent restoration of the LGP32 cytotoxicity to hemocytes (Fig. 3B). Altogether, those results show the essential role of *sodA* in LGP32 resistance to phagocyte killing and subsequent cytotoxicity to hemocytes. However, the Δ*sodA* deletion mutant did not show any significant virulence attenuation in oyster experimental infections (Fig. 3C).

copA is required for copper resistance, intracellular survival and cytotoxicity in phagocytes

Isogenic mutants lacking *cop*A (VS_0768) or *cus*AB (VS_II0515, VS_II0516) were constructed (Supporting Information Fig. S3) to study the role of copper efflux in the intracellular survival and virulence of LGP32. Growth in Zobell medium or plasma and phagocytosis efficiency did not significantly differ from the wild-type LGP32 (Supporting Information Figs S4 and S5). Both deletion mutants were then tested for resistance to copper and zinc (as a control of metal specificity) by zone inhibition assay. Δ*cop*A showed a major increase in susceptibility to copper compared with the wild-type LPGP32, but remained equally susceptible to zinc (Supporting Information Fig. S7). Complementation with a pMRB plasmid carrying *copA* restored resistance to high copper concentrations. No significant difference was observed for the Δ*cusAB* mutant in our *in vitro* assays (Supporting Information Figs S7 and S8). In hemocyte co-cultures, the phagocytosis-dependent growth of LGP32 was strongly attenuated in the Δ*copA* mutant ($P < 0.001$; Fig. 4A). Moreover, the Δ*copA* mutant was two times less cytotoxic than the wild-type LGP32 ($P < 0.001$; Fig. 4B). Importantly, complementation restored the cytotoxicity in hemocytes to wild-type levels (Fig. 4B). This confirmed the essential role of *copA* in LGP32 resistance to copper, intracellular survival and subsequent cytolysis of host cells.

copA i*s required for host colonization and virulence in experimental infections*

In vivo studies were performed to characterize the role of *copA* in LGP32 pathogenesis. In experimental infections of juvenile oysters, the Δ*cop*A mutant showed a significantly attenuated

virulence. Indeed, mortalities at day 7 dropped from 85% for wild-type LGP32 down to 65% ($P < 0.01$) for the Δ*cop*A mutant (Fig. 4C). To investigate the behaviour of the Δ*cop*A mutant *in vivo*, colonization was tested by injecting juvenile oysters with GFP-labelled LGP32 or Δ*copA*. The Δ*copA* mutant showed a significant colonization defect with only 5757 ± 4096 cfu g^{-1} of oyster flesh as opposed to 26 700 ± 4 096 cfu g^{-1} for LGP32 ($P < 0.05$), as soon as 2 h after injection (Fig. 4D). Importantly, confirming our *in vitro* data (Fig. 1B), LGP32 induced a major cytolysis of oyster hemocytes and the release of extracellular bacteria *in vivo* (Fig. 4F), whereas Δ*copA* remained intracellular with most hemocytes showing preserved cell integrity (Fig. 4F). In agreement with the observed Δ*copA* colonization defect, Δ*copA* was massively and significantly ($P < 0.01$) outcompeted by the wild-type LGP32 in co-infection assays where oysters were injected with identical doses of GFP-expressing LGP32 and mCherry-expressing LGP32 or Δ*copA*. We indeed measured very low competitive indexes (CI) = 0.12 ± 0.05 and 0.03 ± 0.05, 2h and 24 h after injection respectively (Fig. 4E). Co-injection of GFP- and mCherry-expressing wild-type LGP32 gave CI∼1 (0.81 ± 0.31 and 1.04 ± 0.31 at 2 h and 24 h, respectively), confirming the absence of bias due to the fluorescent protein expression plasmids used here (Fig. 4E). Altogether, these data show that copper efflux is essential for LGP32 survival in hemocytes, expression of intracellular cytotoxicity, host colonization and virulence in experimental infections.

Discussion

As an increasing number of pathogenic vibrio species have been shown to adopt intracellular stages (Rosenberg and Falkovitz, 2004; Duperthuy *et al*., 2011; Zhang *et al*., 2012; de Souza Santos and Orth, 2014) understanding the mechanisms by which vibrios survive intracellularly has become a priority. Here, we developed a transcriptomic analysis coupled to *in vitro* and *in vivo* functional genomics, through which we identified functions essential for vibrio intracellular survival. Overall, our study provides important insights in several aspects. First, it is to our knowledge the first global characterization of the molecular functions sustaining intracellular life in a vibrio strain whose virulence depends on its intracellular survival in phagocytes. Second, we functionally characterized the antioxidant response and metal homeostasis as two major functions widely conserved among vibrios and essential for vibrio intracellular stages. Third, we identified copper tolerance as a major determinant of vibrio fitness at the host-pathogen interface.

Vibrio tasmaniensis LGP32 was chosen in this study as it has evolved the capacity to survive in oyster hemocytes (Duperthuy *et al*., 2011). Our present study showed that a phagocytosis step was required for LGP32 to finally induce cytolysis of oyster immune cells. Such an intracellular LGP32-driven cytolysis of hemocytes was dependent on LGP32 entry and survival inside hemocytes, as demonstrated with phagocytosis-inhibiting drugs or mutants impaired in intracellular survival. Since

circulating phagocytes were highly damaged in infected oysters, the LGP32-driven cytolysis of oyster hemocytes could cause a dramatic immune suppression of oyster defences promoting pathogenesis.

Oyster hemocytes are immune cells equipped with a complete panel of microbicidal functions (Bachere *et al*., 2015). In particular, they respond to phagocytosis by a rapid and massive oxidative burst highly toxic to phagocytosed microorganisms (Poirier *et al*., 2014). Consistently, the antioxidant response was essential to LGP32 survival in the phagosome hostile environment. *sodA* (VS_2918) and *ahpC*/*ahp*F (VS_2126, VS_2127) were among the genes most highly induced intracellularly. Moreover, MnSOD (*sod*A gene product) was essential for LGP32 intracellular survival and cytotoxicity in oyster phagocytes. By catalysing the conversion of the highly toxic superoxide ion ($O_2^{-\cdot}$) to H_2O_2 and dioxygen (O_2) SODs contribute to tolerance to oxidative stress (Kang *et al*., 2007) and resistance to acidic pH (Kim *et al*., 2005) in diverse vibrio species. In *V. vulnificus*, signals inducing MnSOD expression include low iron and acidic pH (Kim *et al*., 2005), which are signals likely encountered by LGP32 in the phagosome as an active influx of iron and efflux of cations is observed (Supporting Information Table S1).

We report here the essential role of a MnSOD in the intracellular survival of a vibrio species, whereas in the coral pathogen *V. shiloi,* a FeSOD contributes to survival in coral ectodermal cells (Banin *et al*., 2003). Interestingly, in *Escherichia coli*, MnSOD is expressed under ironlimiting conditions, when FeSOD is repressed (Niederhoffer *et al*., 1990). This may explain why MnSOD plays a crucial role in LGP32 intraphagosomal stages, where iron is scarce as indicated by the intracellular activation of iron uptake (Supporting Information Table S1). From our present data and studies on *V. shiloi* (Banin *et al*., 2003), Fe and MnSODs, which share a common ancestor, are required for intracellular survival of at least two pathogenic vibrio species. As they are highly conserved across vibrios, they could be involved in the intracellular survival of additional vibrio species.

One major result of our work is the identification of the essential role of metal homeostasis and copper efflux in particular in vibrio intracellular life and subsequent cytotoxicity, colonization and virulence in oyster experimental infections. However, in the last decade metal homeostasis has been highlighted to play a role in different bacterial pathogenesis in vertebrates (Becker and Skaar, 2014). Among the different metals involved at the host– pathogen interface, the toxicity of copper appears to be mainly used as a defence mechanism by hosts. Hence, copper efflux is an important mechanism for pathogens to avoid copper toxicity. Indeed, free copper enhances the production of reactive oxygen species (ROS) that create damages to a broad series of macromolecules and largely contribute to copper antimicrobial properties (Hodgkinson and Petris, 2012). In H_2O_2-rich environments like the phagosome, the redox properties of Cu(I) catalyse the generation of highly toxic hydroxyl radicals ($OH^{-\cdot}$). Consistent with its major protective role against hemocyte intracellular killing, CopA (VS_0768) of LGP32, a member of the P-type ATPase family exporting Cu(I)

across the plasma membrane (Hodgkinson and Petris, 2012), was highly transcribed in the phagosome. P-type ATPases homologous to CopA have been described in diverse species of intracellular bacteria like *Salmonella* (CopA; Espariz *et al*., 2007) and *Mycobacterium* (CtpV) that invade mammalian phagocytes (Rowland and Niederweis, 2012). As in oyster hemocytes, genes encoding copper-exporting P-type ATPase are upregulated by such pathogens when they enter phagosomes of macrophages (Chaturvedi and Henderson, 2014) in which copper concentration increases up to several hundred micromolar (Wagner *et al*., 2005).

The major role of CopA in LGP32 intracellular survival strongly suggests that phagosomes of oyster hemocytes accumulate copper to control phagocytosed pathogens and supports recent findings showing that both hosts and pathogens manipulate copper content in infected host niches (Chaturvedi and Henderson, 2014; Chaturvedi *et al*., 2014). In particular, mammalian phagocytes have been shown to modulate the intraphagosomal concentration of metals, by depriving microorganisms from essential metals like iron or accumulating toxic metals like copper (Hood and Skaar, 2012). Thus, in human macrophages, metal homeostasis is essential for the control of phagocytosed bacteria (Soldati and Neyrolles, 2012). The main effectors of copper influx in phagosomes of macrophages are CTR1 and ATP7A (Hodgkinson and Petris, 2012) whose expression is essential for the copper-mediated bactericidal activity of the phagosome (White *et al*., 2009). Interestingly, three ATP7A and two CTR1 genes are found in the genome of *Crassostrea gigas* (Genbank accession numbers gbIEKC33905.1, gbIEKC18325.1, gbIEKC28422.1 and gbIEKC31900.1, gbIEKC33878.1). Thus, like mycobacteria replicating inside phagosomes (Neyrolles *et al*., 2015), LGP32 uses copper efflux to resist the high copper concentrations to which it is exposed after phagocytosis. It has been hypothesized that copper detoxification has been conserved during evolution to provide protection against phagocytosis (Raimunda *et al*., 2011; German *et al*., 2013). This hypothesis is supported by the present data, which show that pathogens capable to survive inside phagocytes of invertebrates (here the oyster) use strategies similar to pathogens surviving inside macrophages of vertebrates. This high degree of conservation is consistent with the high conservation of the phagocytotic machinery that intracellular pathogens have to face, from protozoan to metazoan phagocytic cells (Boulais *et al*., 2010). The major role of copper homeostasis at the host– pathogen interface may well go beyond its role in intracellular survival. Indeed, copper efflux was induced as soon as LGP32 entered oyster plasma and was essential for oyster colonization. This is consistent with the copperrich composition of marine invertebrate plasma, which is characterized by abundant copper-containing proteins like Zn/Cu SODs in the oyster (Gonzalez *et al*., 2005; Duperthuy *et al*., 2011) or hemocyanin in crustaceans and cephalopods (Terwilliger and Dumler, 2001) to which squid-colonizing vibrios resist (Kremer *et al*., 2014). A recent study suggested that *cop*A is required for the colonization of the squid light organ by *V. fischeri*

(Brooks *et al*., 2014). We show here for the first time the central role of *cop*A in the pathogenic potential of a vibrio.

The gene *cop*A is highly conserved among vibrios and to a broader extent among bacteria (Hernandez-Montes *et al*., 2012). Hence, copA has been used to evaluate the impact of copper-rich environments on bacterial communities, suggesting that copA is under selection in copperrich environments (Besaury *et al*., 2013). In the wild, copper accumulation often originates from human-related activities and numerous aquatic animals can accumulate copper in their tissues, including oysters (Luo *et al*., 2014). Therefore, copper abundance in different environmental niches, including invertebrates as well as copper of natural or anthropogenic sources, may represent an important driver for the emergence of copper resistant pathogens. In conclusion, this study demonstrates the essential role of copper efflux and antioxidants in vibrio survival inside host cells and suggests that interactions of vibrios with different copper-rich environmental niches could select important adaptive traits favouring emergence of water-borne pathogens.

Experimental procedures

Animals

Adult diploid *C. gigas* were purchased from the local oyster farm in Le Petit Mas (Mèze, France) and used for RNAseq and qRT-PCR analyses. Adult triploid *C. gigas* were purchased from the local oyster farm at the 'CAT de Maguelone' (Palavas, France) to perform *in vitro* cell biology experiments. For experimental infections, juvenile diploid *C. gigas* oysters were provided by the Ifremer oyster hatcheries of Argenton and Bouin (France).

Bacterial strains and culture conditions

Vibrio isolates were grown in Zobell or on Zobell agar (Saulnier *et al*., 2000), Luria-Bertani (LB) or LB-agar (LBA) + NaCl 0.5M, at 20°C. *E. coli* strains were grown in LB or on LBA at 37°C. Chloramphenicol (5–25 μg ml^{-1}), thymidine (0.3 mM) and diaminopimelate (0.3 mM) were added as supplements when necessary. Induction of the P_{BAD} promoter was achieved by the addition of 0.2% L-arabinose to the growth medium, and conversely, repression was obtained by the addition of 1% D-glucose.

Plasmid construction and mutagenesis

Mutagenesis was performed by gene replacement, as described in (Lemire *et al*., 2014). Two independent PCR amplifications of the regions (500 bp) flanking the gene to delete were performed using two primer pairs (1 + 2 and 3 + 4; Supporting Information Table S2). An inside out PCR was performed using the pSW7848T suicide vector DNA (Val *et al*., 2012) and primer pair pSW-F and pSW-R (Supporting Information Table S2). The recombinant plasmid was then assembled by the Gibson assembly method using the Gibson assembly master mix (New England Biolabs, NEB)

according to the manufacturer's instructions. Mutants were screened by PCR using external primer 5 + 6 listed in Supporting Information Table S2. For complementation experiment, the gene of interest was cloned under the control of a constitutive P_{LAC} promoter in a pMRB plasmid (Le Roux *et al*., 2011). Two independent PCR amplifications of the gene and plasmid were performed using the primers gene-*F* + R and *pMRB-F* + *R* reciprocally. After purification and quantification, 100 ng of the PCR products were mixed with the Gibson assembly Master Mix and incubated for 60 min at 50°C. Samples were diluted 1/3 before *E. coli* transformation. Clones were controlled by digestion with restriction enzyme and sequencing of PCR products obtained using the primers described in Supporting Information Table S2. Strains π3813 and β3914 were used as plasmid hosts for cloning and conjugation respectively (Le Roux *et al*., 2007). Conjugation was carried out as described in Goudenège et al., 2014. Plasmids and strains used and/or constructed in the present study are presented in Supporting Information Table S2.

Preparation of vibrios and oyster hemocytes for in vitro *assays*

Hemolymph was collected from the adductor muscle of oysters using a 2 ml syringe with a 23-G needle. After cell counting, freshly collected hemolymph was dispensed in wells to obtain hemocytes monolayers in the desired plate format (see below). In parallel, after growing vibrio strains at 20°C in Zobell medium for 14 h, bacteria were washed in sterile sea water (SSW) by two successive centrifugations (10 min, 1000 *g*, 20°C) and diluted in SSW at a working dilution of 2.10^9cfu ml^{-1} as deduced from OD_{600} reads. When needed, bacteria were opsonized for one hour in 0.22 µm filtered oyster plasma.

In vitro *assay for vibrio intracellular survival*

Hemocytes (2×10^5 hemocytes per well) were plated in Black 96-wells plate with transparent flat bottom and kept in plasma. *Vibrio* strains carrying high copy pMRB-GFP plasmid (Supporting Information Table S2) were opsonised in oyster plasma. Opsonized vibrio strains were then added to the hemocyte monolayers at a multiplicity of infection of 50:1. Binding of bacteria to hemocytes was synchronized by a brief centrifugation of 5 min at 400 *g*. After 1 h of phagocytosis, hemocytes were carefully washed three times with SSW to remove any remaining extracellular bacteria. Then, GFP fluorescence was measured every hour over 20 h using a TECAN plate reader (λex 480 nm/λem 520 nm). In each experiment, each condition was performed in triplicates and the depicted results are the average of three independent experiments. Statistical analysis was performed using RM-ANOVA over the independent experiments.

In vitro *cytotoxicity assay*

Hemocytes (2×10^5 hemocytes per well) were plated in Black 96-wells plate with transparent flat bottom. After 1 h of adhesion and plasma removal, 10 µg ml^{-1} of Sytox Green (Molecular Probes)

diluted in 200 µl SSW was added to each well. Opsonized vibrio strains were then added to the hemocyte monolayers at a multiplicity of infection of 50:1. Binding of bacteria to hemocytes was synchronized by a brief centrifugation of 5 min at 400 *g*. Sytox Green fluorescence was determined (λex 480 nm/λem 550 nm) every 30 min over 14 h using a TECAN microplate reader. For controls, washed bacteria were incubated in Sytox Green diluted in SSW. Maximum cytolysis was determined by incubating hemocytes in Sytox Green in presence of 0.1% Triton X-100. To determine the role of phagocytosis in vibrio-induced cytolysis of hemocytes, hemocytes were incubated with 5 µg ml^{-1} of cytochalasin D, an actin polymerization inhibitor, 30 min before adding vibrios. The results are representative of three independent experiments. The RM-ANOVA test was used to estimate the *P*-values of the comparison.

Fluorescence microscopy

Hemocytes were plated onto glass coverslips in a 24-well plate to obtain monolayers of 5×10^5 cells. After adhesion, hemocytes were exposed to GFP-expressing vibrios (washed in SSW) at a multiplicity of infection of 50:1. Binding of bacteria to hemocytes was synchronized by a brief centrifugation of 5 min at 400 *g*. After 1 h, 3 h and 5 h-incubation time, culture supernatants were fixed with 4% paraformaldehyde for 15 min and cytospun on glass slides for 5 min at 1000 *g*. The cell monolayers (coverslips from bottom of the wells), were also fixed with 4% paraformaldehyde for 15 min. Glass slides and coverslips were then washed in PBS and stained with 0.25 µg ml^{-1} DAPI (Sigma) and 0.5 µg ml^{-1} Phalloidin-TRITC (Sigma). Fluorescence imaging was performed using a Zeiss Axioimager fluorescence microscope and a Zeiss 63× Plan-Apo 1.4 oil objective equipped with a Zeiss MRC black and white camera for image acquisition.

Vibrio transcriptomic analysis by RNAseq

LGP32 was grown at 20°C in Zobell medium for 10 h and washed twice in SSW by centrifugations (10 min, 1000 *g*, 20°C). Bacteria were then resuspended in SSW at OD_{600} of 0.5 (1.10^9 cfu ml^{-1} equivalent). Hemolymph was collected from the adductor muscle of oysters using a 2 ml syringe with a 23-G needle. Freshly collected hemolymph was dispensed in a 6-well plate to obtain monolayers of 6×10^6 hemocytes per well. One hour after plating, vibrios were added at a multiplicity of infection of 100:1, and plates were centrifuged for 5 min at 400 *g* for binding synchronization. After 1 h of co-incubation, wells were washed extensively three times with SSW to remove extracellular bacteria and 500 µl Trizol reagent (Invitrogen) was added to every well for total RNA extraction. The efficiency of vibrios internalization in hemocytes was verified by microscopy showing that about 40% of hemocytes internalized about 50–70 bacteria, with rare bacteria remaining extracellular. As a control, washed bacteria were incubated in triplicates in SSW for 1 h and resuspended in Trizol after centrifugation. RNA from three independent experiments of LGP32 phagocytosis by hemocytes was extracted using the Trizol reagent protocol (Life Technologies). RNA concentration was measured using a NanoDrop 1000 Spectrophotometer (Thermo Fisher Scientific

Inc.) and RNA quality was monitored by agarose gel electrophoresis and a 2100 Bioanalyzer (Agilent Technologies Inc.). The bioanalyser analysis showed that bacterial RNAs represented approximately 10% of the total RNA in the intrahemocyte samples. Accordingly, control samples were prepared by mixing total RNA extracted from LGP32 incubated in SSW with *C. gigas* hemocyte RNA with a ratio of 1:9. For each sample, 7 µg of starting material was treated with DNaseI (4 U) (Ambion's DNA-free™) following the manufacturer's instructions. Samples were then enriched in bacterial RNA using the MICROB*Enrich*™ Kit (Ambion) and bacterial rRNA were then removed by the MICROB*Express*™Kit (Ambion) following the manufacturer's instructions. Because the MICROB*Enrich*™ Kit is based on oligonucleotides that are designed to capture rRNAs from mammal species, it is not fully efficient to remove invertebrate rRNAs. Accordingly, we performed a further depletion step using a 5'-phosphatedependent exonuclease (Terminator, Epicentre), that degrades processed transcripts, following instructions from the manufacturer. For cDNA sequencing, for each sample, a directional cDNA library was constructed and sequenced on an illumina Hiseq 1000, in paired-end reads of 2 × 100 bp. Three samples were multiplexed per lane giving $\sim 60 \times 10^6$ reads per sample. Out of 50–60 M reads obtained from the RNA-seq, 1.2 M reads from the SSW samples and 2.3 M reads from the intrahemocyte samples were successfully mapped onto the genome of LGP32.

Sequencing data analysis

Transcriptomic high throughput sequencing data were analysed using a bioinformatic pipeline implemented in the Microscope platform (Vallenet *et al*., 2013). The current pipeline is a 'Master' shell script that launches the various parts of the analysis (i.e. a collection of Shell/Perl/R scripts) and controls for all tasks having been completed without errors. In a first step, the RNA-Seq data quality was assessed by including option like reads trimming or merging/split pairedend reads. In a second step, reads were mapped onto the *V. tasmaniensis* LGP32 genome (genome ID: 13995, assembly GCA_000091465.1, NCBI) using the SSAHA2 package (Ning *et al*., 2001) that combines the SSAHA searching algorithm (sequence information is encoded in a perfect hash function) aiming at identifying regions of high similarity, and the cross-match sequence alignment programme (Ewing *et al*., 1998), which aligns these regions using a banded Smith-Waterman-Gotoh algorithm (Smith and Waterman, 1981). An alignment score equal to at least half of the read is required for a hit to be retained. To lower false positives discovery rate, the SAMtools (v.0.1.8; Li *et al*., 2009) are then used to extract reliable alignments from SAM formatted files. The number of reads matching each genomic object harboured by the reference genome is subsequently computed with the Bioconductor-Genomic-Features package (Carlson *et al*., 2011). In case of reads matching several genomic objects, the count number is weighted in order to keep the same total number of reads. Finally, the Bioconductor-DESeq package (Anders and Huber, 2010) with default parameters is used to analyse raw counts data and test for differential expression between conditions. Out of the paired-end reads, only mapping results of the first sequencing run reads were used for the DESeq analysis.

qRT-PCR analyses

Experiments were performed as for '*Vibrio* transcriptomic analysis by RNAseq'. Conditions tested were: 6×10^8 vibrios per well in SSW (control), vibrios in oyster plasma and vibrios opsonized in plasma and incubated on hemocyte monolayers (6×10^6 hemocytes per well) kept in SSW. Vibrios were incubated 30 min, 1 h and 2 h before wells were centrifuged and the incubated stopped by adding 500 µl Trizol per well. Total RNA was extracted from Trizol using the DirectZol RNA Miniprep kit (R2051) according to manufacturer's instructions (ZymoResearch) and then treated by DNaseI to remove contaminating genomic DNA, using the DNA-free kit (Ambion) before purification by phenol/chloroform extraction and ethanol precipitation. Quantification of total RNA was done with a NanoDrop spectrophotometer (Thermo, Fisher Scientific) and quality was monitored using a 2100 Bioanalyzer (Agilent Technologies Inc.). Real-time qPCR was performed either at the Imagif platform (Gif sur Yvette) on an ABI 7900HT Fast Real-Time PCR System using a Fast SG qPCR Master Mix (Roboklon), or at the MGX platform in Montpellier using a the Light-Cycler 480 System (Roche), using the primers listed in Supporting Information Table S3. Relative expression was calculated using the 2-ΔΔCq method (Pfaffl, 2001), with three genes, encoding 6PKF (VS_2913), MGS (VS_II1055) and CcmC (VS_0852) being used for normalization. These were chosen because their expression was found to be constant across conditions in the RNAseq, as well as by qRT-PCR.

Copper and zinc sensitivity

Paper discs (6 mm) were loaded with $CuSO_4$ by soaking them over-night into a 50 mM $CuSO_4$ solution or 50 mM ZnSO4 solution. Cells from a stationary phase LGP32 wildtype and LGP32 isogenic mutant cultures at DO = 1 were washed twice with SSW before being spread onto agar plates containing 15 g L^{-1} bactopeptone and 0.5M NaCl. Using a sterile tweezer, copper and zinc impregnated disks were placed on the bacterial lawn before incubation at 20°C. After 5 day incubation, the diameter of the inhibition zone around the disk was measured.

Experimental infections of oysters

Experimental infections were performed at 20°C, as previously described (Duperthuy *et al*., 2010). Groups of 45 oysters were injected with the different strains of LGP32 (4×10^7 cfu per spat). An equal volume of SSW was injected to control animals. Colony-forming units of bacteria were determined by counting on Zobell agar plates. For each condition, oysters were placed for 24 h in three separate tanks in 6 l of seawater (15 animals per aquarium). Mortalities were followed during 7 days. The non-parametric Kaplan–Meier test was used to estimate log-rank values for comparing conditions. All experimental infections were performed according to the Ifremer animal care guidelines and policy.

In vivo *colonization and damages to host cells*

After overnight growth in LB NaCl 0.5M containing 10 µg ml^{-1} chloramphenicol, vibrio strains carrying high copy pMRBGFP were washed twice with sterile sea water (SSW) by centrifugation for 15 min at 1500 *g*. Then, groups of 20 oysters were injected with wild-type or Δ*copA* LGP32 (7×10^7 cfu per oysters). Two hours after injection, hemocytes were collected from the adductor muscle of five oysters and fixed with 2% paraformaldehyde for 15 min and finally cytospun for 5 min at 1000 *g*. Samples were stained with 0.25 µg ml^{-1} DAPI (Sigma) and 0.5 µg ml^{-1} WGA-TRITC (Sigma). Fluorescence imaging was performed as described above. Statistical analysis was performed using non-parametric Mann– Whitney test for comparing both conditions. Similarly, 2 h after injection, five additional oysters injected with each strain were weighed and homogenized by passage through a Dounce apparatus. Serial dilutions of the homogenized material in SSW were spread onto LB NaCl 0.5M agar plates containing 10 µg ml^{-1} chloramphenicol, in duplicate. Colonies were counted after 2 days of growth at 20°C and results were expressed in number of colony forming units per gram of oyster.

In vivo *competitive index*

After overnight growth in LB NaCl 0.5M containing 10 µg ml^{-1} chloramphenicol, wild-type or Δ*copA* LGP32 carrying high copy pMRB-GFP and wild-type LGP32 high copy pMRBmCherry were washed twice in SSW by centrifugation for 15 min at 1500 *g*. Then, groups of 40 oysters were injected with a 1:1 ratio of each strain (7×10^7 cfu per oysters). Two conditions were tested: GFP-wild-type/mCherry-wild-type (control) as well as GFP-Δ*copA*/mCherry-wild-type. Five oysters of each condition were homogenized and plated on agar plates as for the colonization assay. Red colonies (wildtype) and green colonies (mutant) were counted and results were expressed as the ratio of mutant CFUs over wild-type CFUs. Statistical analysis was performed using the nonparametric Kruskal–Wallis test with Dunn's multiple comparisons test for comparing conditions.

Acknowledgements

This study received financial support from the ANR (Vibriogen project, ANR-11-BSV7-0023). We thank Dr Stéphane Cruveiller and Dr Claudine Médigue for RNAseq supervision as well as Dr Julien de Lorgeril and Phillipe Clair for precious advice for qRT-PCR analyses. We thank Bruno Petton and Max Nourry from the Ifremer for providing standardized oyster spat for experimental infections. We thank Marc Leroy for technical assistance. We are indebted to the Montpellier RIO Imaging platform of the University of Montpellier. This work has benefited from the facilities and expertise of the high through put sequencing and the qPCR platforms of IMAGIF (Centre de Recherche de Gif-www.imagif.cnrs.fr).

References

Anders, S., and Huber, W. (2010) Differential expression analysis for sequence count data. *Genome Biol* **11:** R106. Bachere, E., Rosa, R.D., Schmitt, P., Poirier, A.C., Merou, N., Charriere, G.M., and Destoumieux-Garzon, D. (2015) The new insights into the oyster antimicrobial defense: cellular, molecular and genetic view. *Fish Shellfish Immunol* **46:** 50–64.

Banin, E., Vassilakos, D., Orr, E., Martinez, R.J., and Rosenberg, E. (2003) Superoxide dismutase is a virulence factor produced by the coral bleaching pathogen *Vibrio shiloi*. *Curr Microbiol* **46:** 418–422.

Becker, K.W., and Skaar, E.P. (2014) Metal limitation and toxicity at the interface between host and pathogen. *FEMS Microbiol Rev* **38:** 1235–1249.

Besaury, L., Bodilis, J., Delgas, F., Andrade, S., De la Iglesia, R., Ouddane, B., and Quillet, L. (2013) Abundance and diversity of copper resistance genes cusA and copA in microbial communities in relation to the impact of copper on Chilean marine sediments. *Mar Pollut Bull* **67:** 16–25.

Boulais, J., Trost, M., Landry, C.R., Dieckmann, R., Levy, E.D., Soldati, T., *et al*. (2010) Molecular characterization of the evolution of phagosomes. *Mol Syst Biol* **6:** 423.

Brooks, J.F., 2nd, Gyllborg, M.C., Cronin, D.C., Quillin, S.J., Mallama, C.A., Foxall, R., *et al*. (2014) Global discovery of colonization determinants in the squid symbiont *Vibrio fischeri*. *Proc Natl Acad Sci USA* **111:** 17284–17289.

Carlson, M., Pages, H., Aboyoun, P., Falcon, S., Morgan, M., Sarkar, D., and Lawrence, M. (2011). In *GenomicFeatures: Tools for Making and Manipulating Transcript Centric Annotations*. Maintainer, B.P. (ed.). pp. 1–66.

Chaturvedi, K.S., and Henderson, J.P. (2014) Pathogenic adaptations to host-derived antibacterial copper. *Front Cell Infect Microbiol* **4:** 3.

Chaturvedi, K.S., Hung, C.S., Giblin, D.E., Urushidani, S., Austin, A.M., Dinauer, M.C., and Henderson, J.P. (2014) *Cupric yersiniabactin* is a virulence-associated superoxide dismutase mimic. *ACS Chem Biol* **9:** 551–561.

Duperthuy, M., Binesse, J., Le Roux, F., Romestand, B., Caro, A., Got, P., *et al*. (2010) The major outer membrane protein OmpU of *Vibrio splendidus* contributes to host antimicrobial peptide resistance and is required for virulence in the oyster *Crassostrea gigas*. *Environ Microbiol* **12:** 951– 963.

Duperthuy, M., Schmitt, P., Garzon, E., Caro, A., Rosa, R.D., Le Roux, F., *et al*. (2011) Use of OmpU porins for attachment and invasion of *Crassostrea gigas* immune cells by the oyster pathogen *Vibrio splendidus*. *Proc Natl Acad Sci USA* **108:** 2993–2998.

Espariz, M., Checa, S.K., Audero, M.E., Pontel, L.B., and Soncini, F.C. (2007) Dissecting the *Salmonella* response to copper. *Microbiology* **153:** 2989–2997.

Ewing, B., Hillier, L., Wendl, M.C., and Green, P. (1998) Base-calling of automated sequencer traces using phred. I. Accuracy assessment. *Genome Res* **8:** 175–185.

Flannagan, R.S., Cosio, G., and Grinstein, S. (2009) Antimicrobial mechanisms of phagocytes and bacterial evasion strategies. *Nat Rev Microbiol* **7:** 355–366.

German, N., Doyscher, D., and Rensing, C. (2013) Bacterial killing in macrophages and amoeba: do they all use a brass dagger? *Future Microbiol* **8:** 1257–1264.

Gonzalez, M., Romestand, B., Fievet, J., Huvet, A., Lebart, M.C., Gueguen, Y., and Bachere, E. (2005) Evidence in oyster of a plasma extracellular superoxide dismutase which binds LPS. *Biochem Biophys Res Commun* **338:** 1089–1097.

Hernandez-Montes, G., Arguello, J.M., and Valderrama, B. (2012) Evolution and diversity of periplasmic proteins involved in copper homeostasis in gamma proteobacteria. *BMC Microbiol* **12:** 249.

Hodgkinson, V., and Petris, M.J. (2012) Copper homeostasis at the host-pathogen interface. *J Biol Chem* **287:** 13549– 13555.

Hood, M.I., and Skaar, E.P. (2012) Nutritional immunity: transition metals at the pathogen-host interface. *Nat Rev Microbiol* **10:** 525–537.

Kang, I.H., Kim, J.S., and Lee, J.K. (2007) The virulence of *Vibrio vulnificus* is affected by the cellular level of superoxide dismutase activity. *J Microbiol Biotechnol* **17:** 1399–1402.

Kim, J.S., Sung, M.H., Kho, D.H., and Lee, J.K. (2005) Induction of manganese-containing superoxide dismutase is required for acid tolerance in *Vibrio vulnificus*. *J Bacteriol* **187:** 5984–5995.

Kremer, N., Schwartzman, J., Augustin, R., Zhou, L., Ruby, E.G., Hourdez, S., and McFall-Ngai, M.J. (2014) The dual nature of haemocyanin in the establishment and persistence of the squid-vibrio symbiosis. *Proc Biol Sci* **281:** 20140504.

Le Roux, F., Binesse, J., Saulnier, D., and Mazel, D. (2007) Construction of a *Vibrio splendidus* mutant lacking the metalloprotease gene vsm by use of a novel counterselectable suicide vector. *Appl Environ Microbiol* **73:** 777–784.

Le Roux, F., Davis, B.M., and Waldor, M.K. (2011) Conserved small RNAs govern replication and incompatibility of a diverse new plasmid family from marine bacteria. *Nucleic Acids Res* **39:** 1004–1013.

Lemire, A., Goudenege, D., Versigny, T., Petton, B., Calteau, A., Labreuche, Y., and Le Roux, F. (2014) Populations, not clones, are the unit of vibrio pathogenesis in naturally infected oysters. *ISME J* **9:** 1523–1531.

Li, H., Handsaker, B., Wysoker, A., Fennell, T., Ruan, J., Homer, N., *et al*. (2009) The Sequence Alignment/Map format and SAMtools. *Bioinformatics* **25:** 2078–2079.

Luo, L., Ke, C., Guo, X., Shi, B., and Huang, M. (2014) Metal accumulation and differentially expressed proteins in gill of oyster (*Crassostrea hongkongensis*) exposed to long-term heavy metal-contaminated estuary. *Fish Shellfish Immunol* **38:** 318–329.

Ma, A.T., McAuley, S., Pukatzki, S., and Mekalanos, J.J. (2009) Translocation of a *Vibrio cholerae* type VI secretion effector requires bacterial endocytosis by host cells. *Cell Host Microbe* **5:** 234–243.

Neyrolles, O., Wolschendorf, F., Mitra, A., and Niederweis, M. (2015) Mycobacteria, metals, and the macrophage. *Immunol Rev* **264:** 249–263.

Niederhoffer, E.C., Naranjo, C.M., Bradley, K.L., and Fee, J.A. (1990) Control of Escherichia coli superoxide dismutase (sodA and sodB) genes by the ferric uptake regulation (fur) locus. *J Bacteriol* **172:** 1930–1938.

Ning, Z., Cox, A.J., and Mullikin, J.C. (2001) SSAHA: a fast search method for large DNA databases. *Genome Res* **11:** 1725–1729.

Pfaffl, M.W. (2001) A new mathematical model for relative quantification in real-time RT-PCR. *Nucleic Acids Res* **29:** e45.

Poirier, A.C., Schmitt, P., Rosa, R.D., Vanhove, A.S., Kieffer-Jaquinod, S., Rubio, T.P., *et al*. (2014) Antimicrobial histones and DNA traps in invertebrate immunity: evidences in *Crassostrea gigas*. *J Biol Chem* **289:** 24821– 24831.

Raimunda, D., Gonzalez-Guerrero, M., Leeber, B.W., 3rd, and Arguello, J.M. (2011) The transport mechanism of bacterial Cu+-ATPases: distinct efflux rates adapted to different function. *Biometals* **24:** 467–475.

Ritchie, J.M., Rui, H., Zhou, X., Iida, T., Kodoma, T., Ito, S., *et al*. (2012) Inflammation and disintegration of intestinal villi in an experimental model for Vibrio parahaemolyticusinduced diarrhea. *PLoS Pathog* **8:** e1002593.

Rosenberg, E., and Falkovitz, L. (2004) The *Vibrio shiloi/ Oculina patagonica* model system of coral bleaching. *Annu Rev Microbiol* **58:** 143–159.

Rowland, J.L., and Niederweis, M. (2012) Resistance mechanisms of *Mycobacterium tuberculosis* against phagosomal copper overload. *Tuberculosis (Edinb)* **92:** 202–210.

Saulnier, D., Avarre, J.C., Le Moullac, G., Ansquer, D., Levy, P., and Vonau, V. (2000) Rapid and sensitive PCR detection of *Vibrio penaeicida*, the putative etiological agent of syndrome 93 in New Caledonia. *Dis Aquat Organ* **40:** 109– 115.

Smith, T.F., and Waterman, M.S. (1981) Identification of common molecular subsequences. *J Mol Biol* **147:** 195– 197.

Soldati, T., and Neyrolles, O. (2012) Mycobacteria and the intraphagosomal environment: take it with a pinch of salt(s). *Traffic* **13:** 1042–1052.

de Souza Santos, M., and Orth, K. (2014) Intracellular *Vibrio parahaemolyticus* escapes the vacuole and establishes a replicative niche in the cytosol of epithelial cells. *MBio* **5:** e01506–e01514.

Terwilliger, N., and Dumler, K. (2001) Ontogeny of decapod crustacean hemocyanin: effects of temperature and nutrition. *J Exp Biol* **204:** 1013–1020.

Thompson, F.L., Thompson, C.C., and Swings, J. (2003) *Vibrio tasmaniensis* sp. nov., isolated from Atlantic salmon (*Salmo salar* L.). *Syst Appl Microbiol* **26:** 65–69.

Val, M.E., Skovgaard, O., Ducos-Galand, M., Bland, M.J., and Mazel, D. (2012) Genome engineering in *Vibrio cholerae*: a feasible approach to address biological issues. *PLoS Genet* **8:** e1002472.

Vallenet, D., Belda, E., Calteau, A., Cruveiller, S., Engelen, S., Lajus, A., *et al*. (2013) MicroScope – an integrated microbial resource for the curation and comparative analysis of genomic and metabolic data. *Nucleic Acids Res* **41:** D636–D647.

Vanhove, A.S., Duperthuy, M., Charriere, G.M., Le Roux, F., Goudenege, D., Gourbal, B., *et al*. (2015) Outer membrane vesicles are vehicles for the delivery of *Vibrio tasmaniensis* virulence factors to oyster immune cells. *Environ Microbiol* **17:** 1152–1165.

Vidal-Dupiol, J., Ladriere, O., Destoumieux-Garzon, D., Sautiere, P.E., Meistertzheim, A.L., Tambutte, E., *et al*. (2011) Innate immune responses of a scleractinian coral to vibriosis. *J Biol Chem* **286:** 22688–22698.

Wagner, D., Maser, J., Lai, B., Cai, Z., Barry, C.E., 3rd, Honer Zu Bentrup, K., *et al*. (2005) Elemental analysis of *Mycobacterium avium*-, *Mycobacterium tuberculosis*-, and *Mycobacterium smegmatis*-containing phagosomes indicates pathogen-induced microenvironments within the host cell's endosomal system. *J Immunol* **174:** 1491–1500.

White, C., Lee, J., Kambe, T., Fritsche, K., and Petris, M.J. (2009) A role for the ATP7A copper-transporting ATPase in macrophage bactericidal activity. *J Biol Chem* **284:** 33949– 33956.

Zhang, L., Krachler, A.M., Broberg, C.A., Li, Y., Mirzaei, H., Gilpin, C.J., and Orth, K. (2012) Type III effector VopC mediates invasion for *Vibrio* species. *Cell Rep* **1:** 453–460.

Supporting information

Additional Supporting Information may be found in the online version of this article at the publisher's web-site:

Fig. S1. LGP32-induced hemocyte cytolysis and release of bacteria.

Fig. S2. qRT-PCR validation of RNAseq data. **Fig. S3.** PCR validation of gene deletions.

Fig. S4. Growth of LGP32 mutants in liquid growth medium. **Fig. S5.** Phagocytosis of LGP32 mutants by oyster hemocytes.

Fig. S6. Growth in hemocyte co-cultures (A) and cytotoxicity (B, C) of the *ΔahpC* mutant and *ΔahpC Δtsa* double mutant. **Fig. S7.** Increased susceptibility to copper of *ΔcopA* but not *ΔcusAB* mutant.

Fig. S8. Growth in hemocyte co-cultures (A) and cytotoxicity (B) of the *ΔcusAB* mutant.

Table S1. Differential expression of LGP32 transcripts from RNAseq data.

Table S2. Strains, plasmids and oligonucleotides. **Table S3.** Oligonucleotides for qRT-PCR.

Fig. 1. Hemocyte phagocytosis and cytolysis support efficient replication of LGP32.

A. Phagocytosis-dependent growth of LGP32 in hemocyte co-cultures. In three independent experiments, hemocyte monolayers wereincubated at a MOI of 50:1 with LGP32 or the avirulent control LMG 20012^{T}. In controls, vibrios were incubated in SSW in the absence of hemocytes. Growth was monitored by the fluorescence of the GFP-expressing bacteria. Values are presented ± SEM ***$P < 0.001$ (two-way rANOVA).

B. LGP32-induced hemocyte cytolysis and extracellular release of bacteria. Monolayers of hemocytes infected at a MOI of 50:1 withGFP-expressing LGP32 or LMG20012^{T} were observed 1 h and 5 h after contact. Both strains were rapidly phagocytosed. Major hemocyte lysis and release of extracellular vibrios was observed after 5 h upon exposure to LGP32 but not LMG 20012^{T}. Nuclei were stained with DAPI and actin cytoskeleton with phalloidin-TRIC. Scale bar: 5 µm.

C. Phagocytosis-dependent cytolysis of hemocytes. Hemocyte monolayers were incubated with LGP32 or LMG 20012^{T} at a MOI of 50:1 for phagocytosis in the presence/absence of cytochalasin D. Hemocyte cytolysis was monitored by using cell impermeant Sytox green DNA dye. The percentage of hemocyte lysis was obtained by comparison with a Triton X100-incuded lysis (100% lysed hemocytes). Values are presented ± SEM. **$P < 0.01$ (RM-ANOVA).

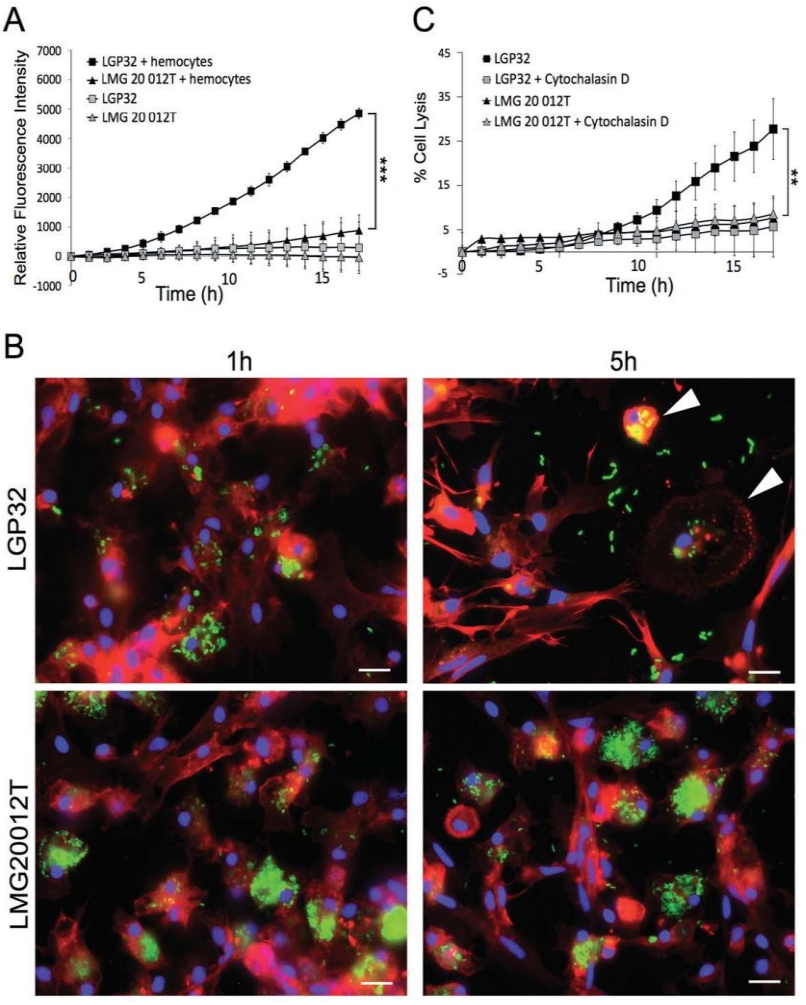


Figure 2

Time-course of LGP32 antioxidant and copper efflux gene expression monitored by qRT-PCR. Vibrio gene expression was analysed for every time point in three independent experiments. Conditions included vibrios in SSW (control), vibrios in oyster plasma (opsonization) and intracellular vibrios in oyster hemocytes. Three incubation times were tested (30 min, 1 h, 2 h). Relative expression was calculated by normalization using three constitutively expressed genes VS_2913, VS_0852 and VS_II1055. Results were standardized relative to the control condition (vibrios in SSW). Data are the mean of gene expression in the three independent experiments ± SEM. Data were analysed by two-way ANOVA and Tukey's post-test for multiple comparison, *P < 0.05, **P < 0.01, ***P < 0.001.

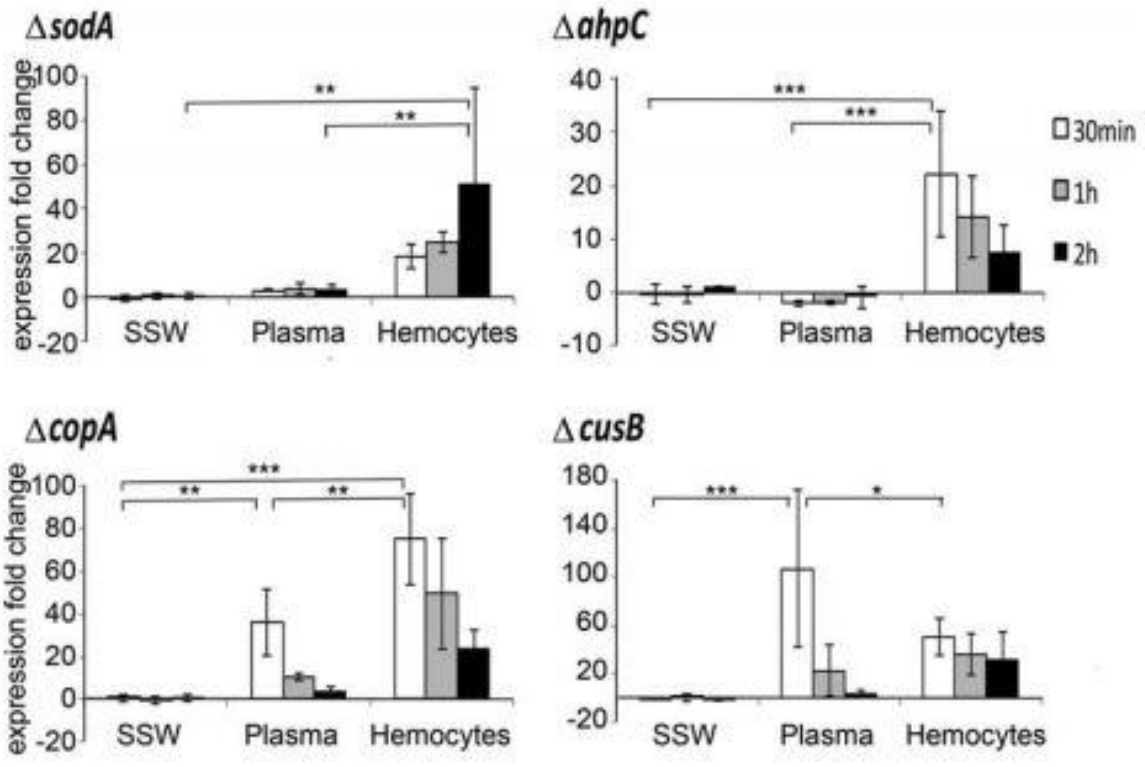


Figure 3

sodA is required for intracellular survival and cytotoxicity in phagocytes. In three independent experiments, hemocyte monolayers were incubated at a MOI of 50:1 with LMG 20012T (control), wild-type LGP32 or its ΔsodA isogenic mutants complemented or not with a low or high copy plasmid carrying sodA. A. Phagocytosis-dependent growth of LGP32 was monitored by the fluorescence of the GFP-expressing bacteria.

***P < 0.001 (RM-ANOVA). B. Cytotoxicity to hemocytes was monitored by the Sytox green assay. Values are presented ± SEM.

**P < 0.01;

*P < 0.05 (RM-ANOVA). C. Kaplan–Meier survival curves were generated from oysters injected with 4 × 107 cfu per animal of the wild-type LGP32 or the ΔsodA isogenic mutant. An injection of sterile seawater (SSW) was used as control. Groups of 45 oysters (15 per seawater tank) were monitored for 7 days after infection. One experiment representative of three independent experiments is shown.

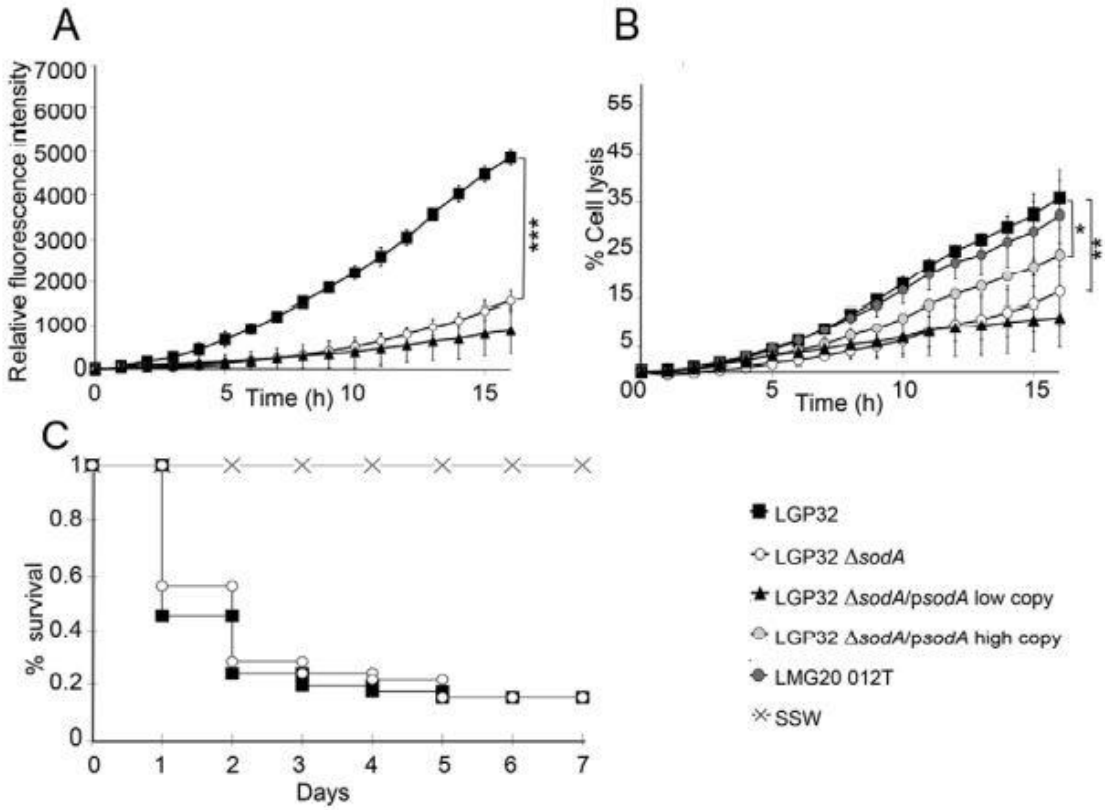


Figure 4

copA is required for intracellular survival, cytotoxicity in phagocytes, host colonization and virulence. Phagocytosis-dependent growth (A), cytotoxicity (B) and virulence (C) of bacteria were monitored. In (C), Kaplan–Meier survival curves were generated from oysters injected with 4 × 107 cfu per animal of the wild-type LGP32 or the ΔcopA isogenic mutant. One experiment representative of three independent experiments is shown. **P < 0.05 (log-rank test). Colonization (D) and competitive indexes (E) were tested by injecting juvenile oysters with fluorescent vibrios at 7 × 107 cfu per oyster and counting cfus from total oyster flesh either 2 h or 24 h after injection. Each dot represents one animal. For competitive indexes (E), the ratio between GFP-expressing ΔcopA and mCherry-expressing LGP32 is shown in white boxes while the ratio between GFP-expressing LGP32 and mCherry-expressing LGP32 is shown in black boxes. For photographs of oyster hemolymph containing GFP-labelled vibrios 2 h after injection (F), oyster hemolymph was cytospun on a glass slide and stained with DAPI and TRITC-WGA. Arrowheads indicate LGP32 associated with cell debris.

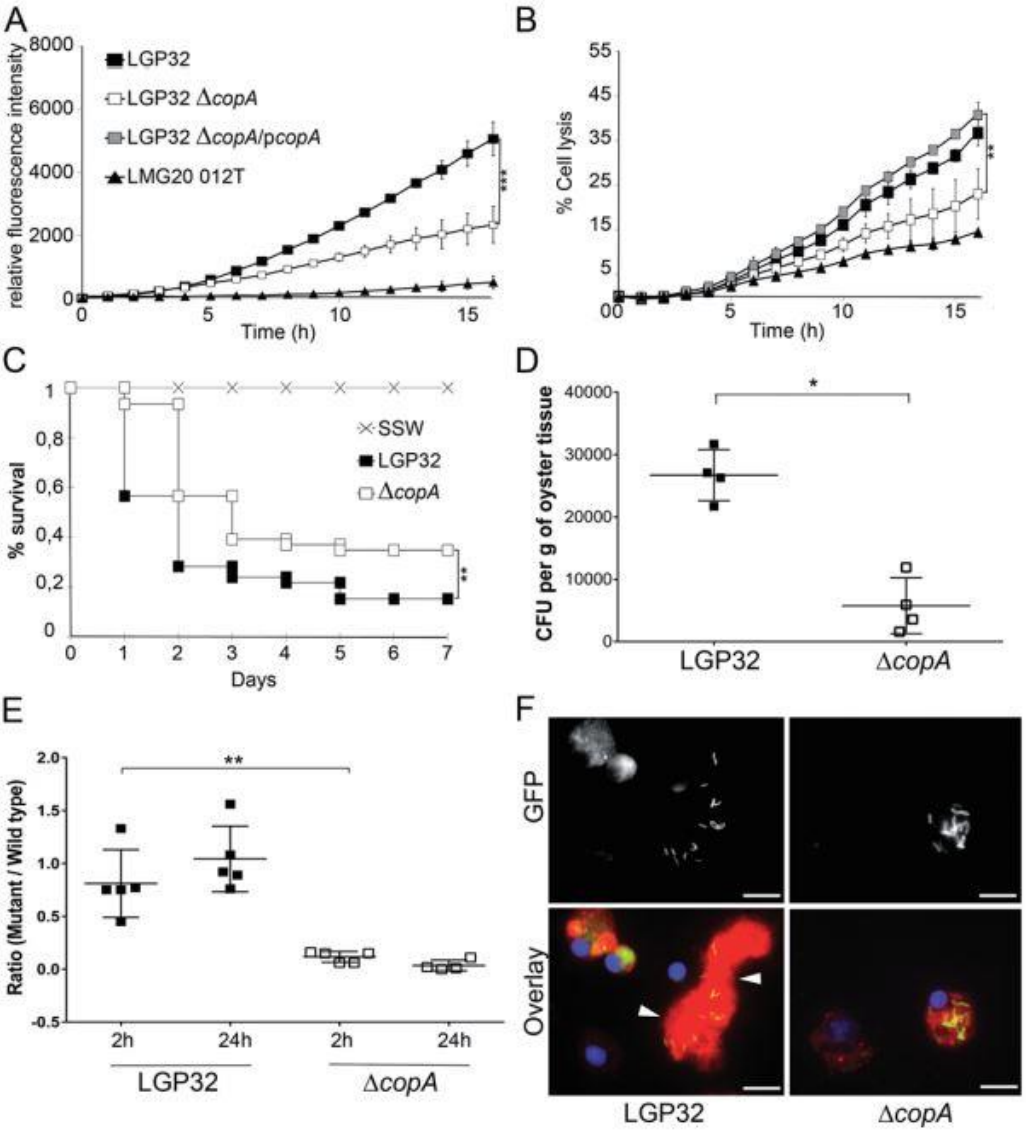


Table 1

Functional categories referring to gene transcripts over/sub-represented in the intracellular condition

Functional category	Number of genes
Protein synthesis	105/12
Carbon compound utilization and transport	83/31
Amino acid metabolism and transport	93/19
Transport (others)	22/41
Energy production and respiration	34/28
Stress response	25/32
Metal homeostasis	39/9
Nucleoside and nucleotide metabolism	30/5
Cofactor and small molecule carrier biogenesis	23/8
DNA replication, recombination and repair	21/9
Signalization	8/21
LPS and capsule biogenesis	21/7
Pilus biogenesis	18/10
Glycolysis/gluconeogenesis/TCA cycle	26/1
Virulence	10/13
Envelope biogenesis	15/6
Fatty acid and phospholipid metabolism	12/9
Central intermediary metabolism	13/3
Transcriptional regulation	6/7
Chemotaxis	9/3
Mobile genetic elements	0/11
Protein and peptide degradation	5/5
Cell division	6/0
DNA metabolism	2/3
Transcription	3/1
Motility	3/0

Table 2

List of the 34 transcripts enriched by more than 50 times in the intracellular condition.

Label	Product	log2 fold change
VS_II0905	Putative endoribonuclease, translation inhibitor	9.49
VS_II0514	**Copper efflux outer membrane protein, *cusC***	**9.2**
VS_II0517	Periplasmic copper-binding protein, *cusF*	8.15
VS_II0904	Aldehyde dehydrogenase	7.65
VS_1283	Conserved hypothetical protein	7.26
VS_II0149	Phospholipase	6.96
VS_II1062	Secreted metalloprotease PrtV/InhA *prtV*	6.94
VS_2126	**Alkyl hydroperoxide reductase subunit C, *ahpC***	**6.9**
VS_2127	Alkyl hydroperoxide reductase subunit F, *ahpF*	6.84
VS_II0515	**Copper efflux membrane fusion protein, *cusB***	**6.76**
VS_1282	Putative methylcobalamin:homocysteine methyltransferase, *metE*	6.73
VS_2591	Maltodextrin transport system permease protein, *malC*	6.58
VS_1145	5-methyltetrahydropteroyl triglutamate-homocysteine methyltransferase	6.55
VS_1068	Outer membrane protein	6.39
VIBSP2_misc_RNA_19	IGR VS_II0219-VS_II0220, *vsr217*	6.37
VS_2589	Cytoplasmic membrane-associated tetrahaem c-type cytochrome, *cymA*	6.33
VS_3121	Phosphoribosylaminoimidazole carboxylase ATPase subunit, *purK*	6.33
VS_0992	Oligopeptide transport system permease protein *oppC*	6.28
VS_2246	Putative succinate dehydrogenase, flavoprotein subunit	6.13
VS_1313	Putative tricarboxylate transport, *tctC*	6.12
VS_2244	succinate dehydrogenase, *sdhB*	6.06
VS_II0903	Putative dipeptidase	6
VS_1461	Cytochrome c oxidase subunit, *ccoQ*	5.93
VS_2585	Cyclomaltodextrin glucanotransferase precursor	5.92
VS_0768	**Copper-exporting *P*-type ATPase A, *copA***	**5.87**
VS_0175	Cold shock protein, *cspA*	5.84
VS_1967	Anthranilate synthase beta subunit, *trpD*	5.81
VS_2927	Aspartate carbamoyltransferase, catalytic chain, *pyrB*	5.72
VS_II0545	Putative glycine betaine transporter, *betT*	5.71
VS_2382	D-methionine transport ATP-binding protein, *metN*	5.7
VS_2241	Succinyl-CoA synthetase beta chain, *sucC*	5.7
VS_II0516	**Copper efflux membrane component, *cusA***	**5.69**
VS_2918	**Superoxide dismutase, *sodA***	**5.69**
VS_2242	Dihydrolipoyllysine-residue succinyltransferase	5.66

See Supporting Information Table S1 for extensive list of differentially represented transcripts. Genes characterized in the present study are in boldface.